Applied Catalysis B: Environmental 302 (2022) 120837

Contents lists available at ScienceDirect

Applied Catalysis B: Environmental

journal homepage: www.elsevier.com/locate/apcatb

# Water accelerates and directly participates soot oxidation: An isotopic study

Weinan Yang [a], Ya Wang [a], Houlin Wang [a], Yani Zhang [a], Yue Peng [a,*], Junhua Li [a,*]

[a] State Key Joint Laboratory of Environment Simulation and Pollution Control, School of Environment, Tsinghua University, Beijing 100084, China

ARTICLE INFO

*Keywords:*
Soot oxidation
Water
Isotope
Manganese oxide

ABSTRACT

Water vapor is inevitable in automobile exhaust and its influence on soot oxidation is of great interests to many researchers. In this paper, we utilized heavy-oxygen water ($H_2{}^{18}O$) to investigate the water participation extent and its relationship with soot oxidation activity. By comparing the quantity of labeled species in products, we noticed water participated in both bare and catalytic soot oxidation. The tighter contact between soot and catalyst, the more involvement of water. But the extent was not affected by the redox property of $Mn_2O_3$ catalysts. The promotional effect of water on activity was observed in all investigated conditions, which was probably because water could be dissociated to more active oxygen species and accelerate the regeneration of oxygen vacancies. But hydrogen atoms left by water still need to be eliminated by dioxygen. Hence in general water worked as an accelerator rather than oxidant.

## 1. Introduction

Soot, emitted by gasoline or diesel engines, is one of the major sources of primary particles, which not only restrict the visibility but also irritate human respiratory system [1–3]. Particulate filter is an effective apparatus to reduce soot emission. The accumulated soot particles need to be combusted periodically to decrease the back pressure of systems, prevent plugging and maintain the economic efficiency. Catalysts could be coated onto the filter to facilitate soot oxidation [4–6].

The different soot oxidation routes under dry conditions have been visualized in the inner rectangle in Scheme 1. For bare soot oxidation, it takes three steps: Step A1, the adsorption and dissociation of molecular oxygen on soot surface, which produces active oxygen species (AOS). Step A2, the formation of surface-oxygen complexes (SOCs), owning to the reaction between AOS and free active carbon site on soot surface. And finally Step A3, the decomposition of SOCs. SOCs contain various kinds of functional groups, the ones with lactone, carboxylic or anhydride groups decompose to generate more $CO_2$, while the others with carbonyl, phenol, ether or quinone groups produce more CO [7–9]. A1-A3 take place on the surface of soot, as shown in the greenish region. For catalytic reaction, the activation energy for gas adsorption and dissociation will be greatly reduced, as the surface of catalysts harbor lots of surface defects like oxygen vacancies. Such defects are prone to adsorb molecular oxygen and could facilitate its dissociation. Short-range AOS produced from the adsorption and dissociation of $O_2$ will be involved in the catalytic reaction on the interface of soot and catalyst (B1), as displayed in the yellowish region, where the SOCs are formed locally (B2) and decompose subsequently (B3). Moreover, the surface of catalyst not in direct contact with soot (the bluish region) cloud also help to yield distant AOS. Unlike close AOS, the distant ones have to migrate to the interface of soot and catalyst (C1) or/and the further soot surface (C2) to form SOCs.

In traditional view, the oxidizing gases, such as $O_2$, $NO_2$ are considered as the active gases. Hence the derived surface AOS, such as $O^-$, $O_2^-$, $O_2^{2-}$, etc., do not include hydrogen atoms [10]. However, the exhaust of gasoline or diesel engines consists of large amount of water vapor. Therefore, it is necessary to determine its participation extent, and to evaluate its effect on soot oxidation activity. Such problems in other environmental catalytic oxidation reactions have been studied extensively, such as CO oxidation [11–13], formaldehyde oxidation [14,15], and halocarbon oxidation [16–18]. However, in soot oxidation, the questions still require systematically investigation. The effect of water on soot oxidation activity was controversial according to different researchers. Some observed promotional effect after addition of water [19–22,23], although the promotion extent varied with the atmosphere composition and contact condition. Generally, the increase was attributed to the gasification of carbon with water and the formation of nitric and nitrous acids when $NO_2$ exists. However, the inhibiting effect was also reported because the competitive adsorption of water and NO hindered NO oxidation [24]. The participation of water was evidenced by Chung Sun Park et al. with the help of $H_2{}^{18}O$ [25]. But they only

* Corresponding authors.
*E-mail addresses:* pengyue83@tsinghua.edu.cn (Y. Peng), lijunhua@tsinghua.edu.cn (J. Li).

https://doi.org/10.1016/j.apcatb.2021.120837
Received 19 July 2021; Received in revised form 26 September 2021; Accepted 17 October 2021
Available online 20 October 2021

considered the tight contact condition and found that under such conditions all $CO_x$ products had been labeled. The more detailed influencing factors remain to be investigated.

The traditional catalyst of soot oxidation is nobel metal catalyst, such as $Pt/Al_2O_3$. However, as reported in our previous research, under lean $O_2$ condition, $Pt/Al_2O_3$ exhibited poor catalytic activity and selectivity [26]. Manganese based oxide has been studied widely as a potential substitute of nobel metal catalyst because it is highly active and environmental benign [27]. Apart from CO oxidation [28–30], methane oxidation [31,32], non-methane hydrocarbon combustion [33–36,37], manganese oxide has been also applied in soot oxidation [38,39]. In our precedent research, $\alpha$-$Mn_2O_3$ synthesized by selective dissoluting $LaMnO_3$ presented sponge-like morphology with disorder-interconnected mesopores and exhibited better soot oxidation activity and selectivity [26].

Hence, in present work, we utilized the same selective dissolution method to synthesize the catalysts, conducted the isotopic soot oxidation experiments, investigated the determining factors (i.e., contact condition, atmosphere composition, and the redox properties of catalysts) influencing water's participation extent under various conditions, and further discussed its relationship with soot oxidation activity.

## 2. Experimental

### 2.1. Materials and synthesis

The preparation of catalysts used in this work has been described in our previous publications [26]. In general, perovskite lanthanum manganese oxide ($LaMnO_3$) was synthesized via citrate sol-gel process. Then dilute $HNO_3$ was utilized to selective dissolute $La^{3+}$ from perovskite and leave out $\gamma$–like $MnO_2$, which was further calcined at 500 ˚C or 800 ˚C for 5 h to produce $Mn_2O_3$–500 and $Mn_2O_3$–800 respectively. Printex-U, a kind of commercial carbon black bought from Degussa, Germany was used as soot surrogate. Heavy-oxygen water ($H_2{}^{18}O$, 99 atom% $^{18}O$) was purchased from Energy Chemical.

### 2.2. Characterization of catalyst properties

#### 2.2.1. Phase structure

The phase structure was determined by powder X-ray diffraction (XRD) patterns, which were collected on Rigaku D/max 2500V X-ray diffractometer under continuous mode with the speed of 10˚/min from 10˚ to 90˚. Raman spectra were collected on Renishaw inVia Reflex Raman spectrometer with a green 532 nm/50 mW diode pumped solid state laser. The Raman shift range was between 500 and 850 $cm^{-1}$ with 1.2 $cm^{-1}$ spectral resolution.

#### 2.2.2. Redox properties

The redox property was investigated by hydrogen temperature programmed reduction ($H_2$-TPR) and oxygen temperature programmed desorption ($O_2$-TPD) experiments. Both experiments were conducted on Micromeritics AutoChem II +2920. For $H_2$-TPR, about 25 mg catalyst was pretreated in 50 mL/min Ar at 300 ˚C for 1 h. Then the degassed catalyst was treated in 50 mL/min 5% $H_2$/Ar and heated to 850 ˚C at a ramping rate of 10 ˚C/min. For $O_2$-TPD, about 50 mg catalyst was degassed in the same condition as the degas step in $H_2$-TPR. The degassed sample was treated in 50 mL/min 5% $O_2$/He for 1 h. After being flushed with 50 mL/min He at room temperature for 30 min, the sample was heated to 850 ˚C at a ramping rate of 10 ˚C/min. During the process, TCD signal, time and temperature were recorded.

### 2.3. Soot-TPO, soot-ISO, and isotopic study

#### 2.3.1. Experimental set-up

Temperature programmed oxidation of soot (soot-TPO) under various reaction conditions were conducted to investigate the activity, selectivity and water influence of soot oxidation process, as listed in Table 1. The catalysts and soot were blended in two different ways to achieve loose contact (LC) and tight contact (TC) conditions. For LC, 10 mg soot and 50 mg catalyst were mixed with a spatula for 2 min. But for TC, the same amount of soot and catalyst were milled together using mortar for equal time. The both mixture were further diluted with 300 mg silica to minimize the effect of hot spots following the same procedure as LC. Then the sample was supported on a bed of quartz wool (around 3 mm in height) in a vertical reactor with a diameter of 11 mm.

**Table 1**
Soot oxidation performance under different reaction conditions.

| Reaction# | [$^{16}O_2$] | [$H_2{}^{18}O$] | Catalyst | Contact Mode | $T_{50}$ (˚C) | $S_a$ (%) |
|---|---|---|---|---|---|---|
| R#1 | 1% | – | – | – | 692 | 22 |
| R#2 | | | $Mn_2O_3$- | LC | 619 | 94 |
| R#3 | | | 500 | TC | 423 | 95 |
| R#4 | 1% | 3% | – | – | 683 | 30 |
| R#5 | | | $Mn_2O_3$- | LC | 608 | 94 |
| R#6 | | | 500 | TC | 385 | 94 |
| R#7 | | | $Mn_2O_3$- | LC | 638 | 90 |
| R#8 | | | 800 | TC | 462 | 91 |
| R#9 | 5% | 0.7% | $Mn_2O_3$- | LC | 572 | 92 |
| R#10 | | | 500 | TC | 391 | 95 |

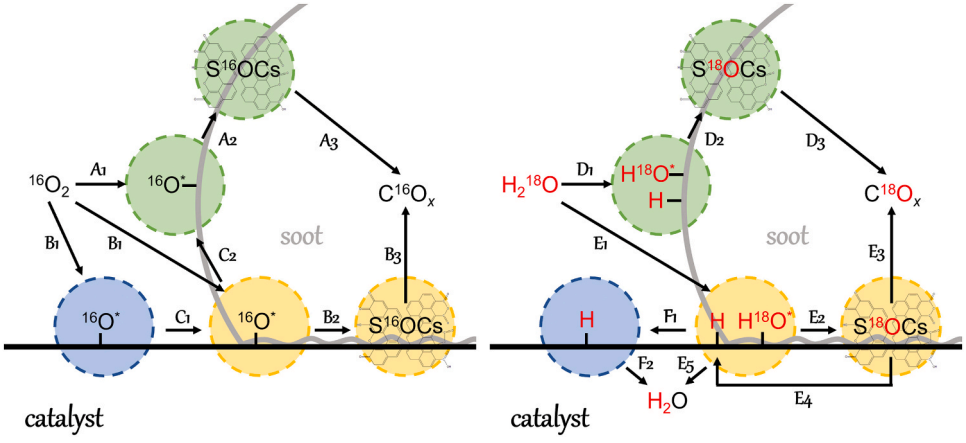


**Scheme 1.** The simplified scheme of soot oxidation routes. The three colored regions represent three types of interfaces where active gases are adsorbed, dissociated and reacted: the surface of soot (the greenish region), the interface between soot and catalyst (the yellowish region) and the surface of catalyst (the bluish region). The arrows with labels represent the intermediate steps for each soot oxidation route. O* and HO* represent two kinds of adsorbed AOS.

The active gases ($^{16}O_2$ and $H_2{}^{18}O$) were balanced with Helium, and the total flow rate equaled 500 mL/min, equivalent to a 600,000 $mLg^{-1}\ h^{-1}$ weight hourly space velocity (WHSV) or 320,000 $h^{-1}$ gas hourly space velocity (GHSV). Water was injected into a 320 ˚C gasification chamber with a 10 μL/min injection speed before it was blended with other gases. After introducing the gases, the reactor was heated to 150 ˚C, hold for 30 min and then reheated to 850 ˚C with a ramping rate of 10 ˚C/min.

Isothermal soot oxidation experiments (soot-ISO) were conducted to evaluate the reaction activity excluding the influence of adsorption and desorption. The sample preparation and pretreatment procedures were the same as soot-TPO. Then the samples were reheated to 250 ˚C and hold for 30 min. Then heated to 300 ˚C and hold another 30 min.

#### 2.3.2. Data recording and processing

Mass spectrometer (HPR-20 R&D, Hiden Analytical) was employed to monitor the concentration of several gases. The mass spectrometer used electron ionization method and the ionization energy was set to 70 eV. The following mass-to-charge ratios ($m/z$) have been recorded: 18, 20, 28, 30, 44, 46 and 48, which could be ascribed to $H_2{}^{16}O$, $H_2{}^{18}O$, $C^{16}O$, $C^{18}O$, $C^{16}O_2$, $C^{16}O^{18}O$, and $C^{18}O_2$ respectively. According to the standard fragmentation patterns of $CO_2$ in NIST Chemistry WebBook, the signal intensity of $m/z = 28$ is around 10% of that of $m/z = 44$. Thus the signal recorded at $m/z = 28$ and 30 contained the fragmentation of $C^{16}O_2$, $C^{16}O^{18}O$ and $C^{18}O_2$, and calculated $CO_2$ selectivity ($S_a$) was lower than actual value. But this deviation did not influence the qualitative comparison between various reaction conditions.

The obtained original soot-TPO profiles are the partial pressure of certain gases varying with temperature. Here we listed the equations used to process original data.

Calculation of soot conversion:

$$Conversion = \frac{\int_{T_l}^{T_i}([C^{16}O] + [C^{18}O] + [C^{16}O_2] + [C^{16}O^{18}O] + [C^{18}O_2])}{\int_{T_l}^{T_h}([C^{16}O] + [C^{18}O] + [C^{16}O_2] + [C^{16}O^{18}O] + [C^{18}O_2])} \times 100\% \quad (1)$$

where $T_l$ is 200 ˚C; $T_h$ is 800 ˚C; $T_i$ is present temperature; [$CO_x$] is the instant concentration of corresponding $CO_x$ species, here we used the partial pressure directly without further converting. The meaning of the parameters are the same in following equations. Calculation of average selectivity ($S_a$):

$$S_a = \frac{\int_{T_l}^{T_h}([C^{16}O] + [C^{18}O])}{\int_{T_l}^{T_h}([C^{16}O] + [C^{18}O] + [C^{16}O_2] + [C^{16}O^{18}O] + [C^{18}O_2])} \times 100\% \quad (2)$$

Calculation of the percentage of $^{18}O$ in reactants ($P_r$):

$$P_r = \frac{\left[H_2^{18}O\right]_{T_l}}{2\left[^{16}O_2\right]_{T_l} + \left[H_2^{18}O\right]_{T_l}} \times 100\% \quad (3)$$

Calculation of the percentage of $^{18}O$ in CO ($P_m$):

$$P_m = \frac{\int_{T_l}^{T_h}[C^{18}O]}{\int_{T_l}^{T_h}([C^{16}O] + [C^{18}O])} \times 100\% \quad (4)$$

Calculation of the percentage of $^{18}O$ in $CO_2$ ($P_d$):

$$P_d = \frac{\int_{T_l}^{T_h}([C^{16}O^{18}O] + 2[C^{18}O_2])}{\int_{T_l}^{T_h}2([C^{16}O_2] + [C^{16}O^{18}O] + [C^{18}O_2])} \times 100\% \quad (5)$$

Calculation of the percentage of $^{18}O$ in all products ($P_p$):

$$P_p = \frac{\int_{T_l}^{T_h}\left([C^{18}O] + \left[C^{16}O^{18}O\right] + 2[C^{18}O_2]\right)}{\int_{T_l}^{T_h}\left([C^{16}O] + [C^{18}O] + 2[C^{16}O_2] + 2[C^{16}O^{18}O] + 2[C^{18}O_2]\right)} \times 100\% \quad (6)$$

### 2.4. Computational details

The adsorption energy ($E_{ad}$) for $O_2$ and $H_2O$ on $Mn_2O_3$ (111) were calculated via density functional theory (DFT) method. All the structural relaxation were performed by using Vienna Ab Initio Simulation Package (VASP) [40,41]. The generalized gradient approximation (GGA) with the Perdew-Burke-Ernzerhof (PBE) [42] exchange correlation function was employed. Besides, DFT+U method with a Hubbard-like term ($U_{eff}$) [43], 4.0 eV was also applied for Mn [44]. The energy cut-off was set as 400 eV, and only the Gamma point mesh was used for Brillouin zone integration. The $Mn_2O_3$ (111) clean and oxygen vacancy models were established in Fig. 1. The former one, denoted as top-site, represents the majority sites on $Mn_2O_3$ (111) surface. $E_{ad}$ can be calculated as follows:

$$E_{ad} = T_{S+X} - T_X - T_S \quad (7)$$

where $T_{S+X}$ denotes the total energy for the complex including $Mn_2O_3$(111) slab model and compound (i.e., $O_2$ or $H_2O$). $T_X$ and $T_S$ represent the total energies for the compound and the slab model, respectively.

## 3. Results and discussion

### 3.1. Catalyst properties

The normalized XRD patterns in Fig. 2(a) reflect the phase structure of as-prepared samples. The patterns of precursor $LaMnO_3$ prepared by citrate sol-gel method were in agreement with PDF#86–1234 $La_{0.96}Mn_{0.96}O_3$, and that of $Mn_2O_3$-500 and $Mn_2O_3$-800 were in consistent with PDF#41–1442 $Mn_2O_3$. Also as shown in the picture, the rougher patterns and the wider peaks of $Mn_2O_3$-500 meant that its crystal size was smaller than that of $Mn_2O_3$-800. The $N_2$-sorption profiles showed that although the isotherm of $Mn_2O_3$-500 was more typical than $Mn_2O_3$-800, both samples exhibited Type IV isotherms and Type H3 hysteresis loop, which was a characteristic of mesoporous structure. The Barrett-Joyner-Halenda (BJH) plot in Fig. 2(c) confirmed the result that pore sizes of $Mn_2O_3$-500 and $Mn_2O_3$-800 centered at 18 nm and 78 nm respectively. The redox properties were examined by $H_2$-TPR and $O_2$-TPD. Both samples had two $H_2$ reduction peaks, as shown in Fig. 2 (d), but the temperatures of $Mn_2O_3$-500 (300 ˚C) was much lower than that of $Mn_2O_3$-800 (378 ˚C). Besides, the total $H_2$ consumption of the latter one was 7.5 $mmol/g_{cat}$, higher than that of $Mn_2O_3$-800 (6.9 $mmol/g_{cat}$). The results of $O_2$-TPD displayed in Fig. 2(e) also support the conclusion that $Mn_2O_3$-500 had more sites to generate AOS and exhibited better redox property because it released more $\alpha$'-O in 300–500 ˚C. As shown in Fig. 2(f), the Raman spectra of $Mn_2O_3$-500 and $Mn_2O_3$-800 were quite similar with the same main peak at 647 $cm^{-1}$, which corresponds to the symmetric stretch vibration mode[45].

### 3.2. DFT calculation

$E_{ad}$ for $H_2O$ on the top site of $Mn_2O_3$(111) is −0.81 eV, which is stronger than that for $O_2$ (−0.60 eV). It indicates that $H_2O$ molecule is easier to be adsorbed onto the top site of $Mn_2O_3$(111) than $O_2$. However, for the oxygen vacancy site of $Mn_2O_3$(111), the $E_{ad}$ of $H_2O$ is −1.23 eV, which is slightly higher than that for $O_2$ (−1.26 eV). This shows that the oxygen vacancy can promote the adsorption for both $O_2$ and $H_2O$ towards $Mn_2O_3$(111), and the enhancement effects for $O_2$ is stronger than that for $H_2O$.

### 3.3. Soot oxidation under dry conditions

The soot oxidation activity and selectivity under different reaction conditions have been listed in Table 1. As displayed in Table 1, R#1 – R#3 were conducted under dry conditions where oxygen concentration

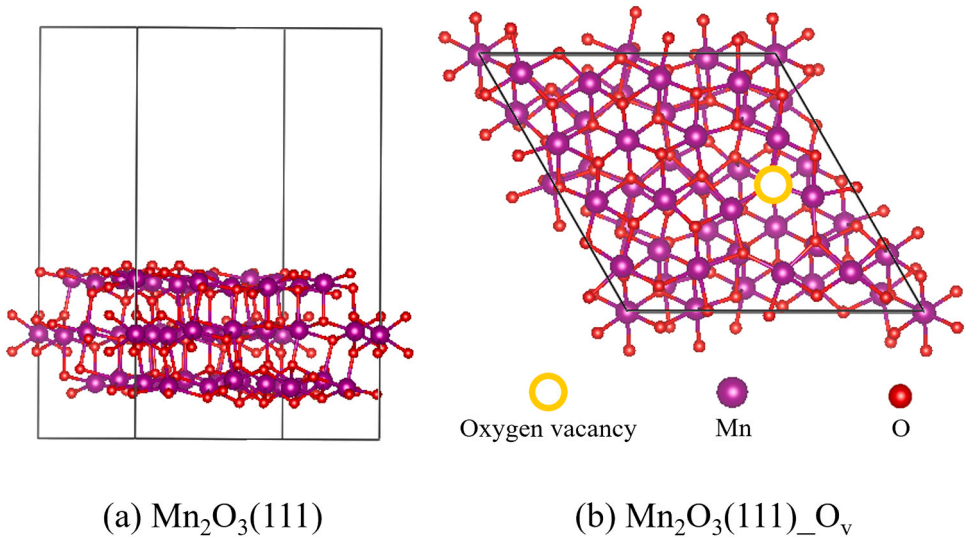


**Fig. 1.** The slab models for (a) $Mn_2O_3$(111) and (b) $Mn_2O_3$(111) with an oxygen vacancy.

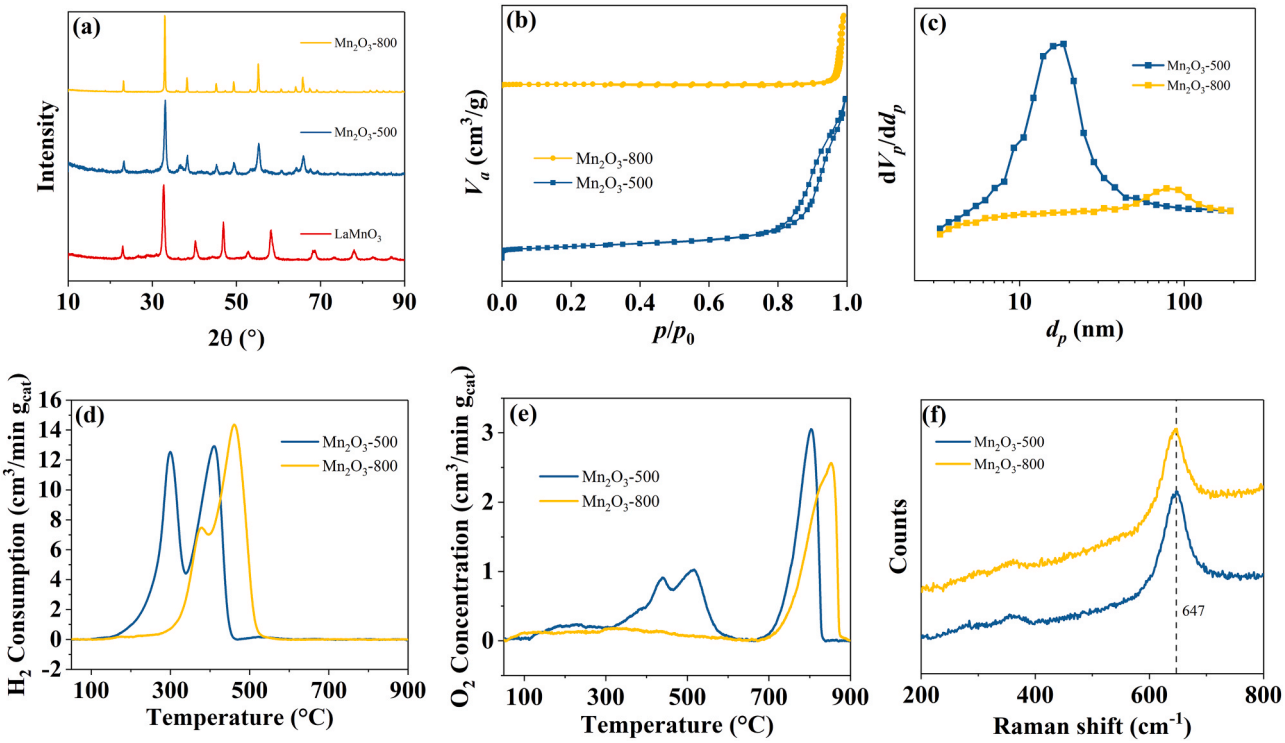


**Fig. 2.** The properties of catalysts. (a) XRD; (b) $N_2$-sorption profiles; (c) BJH plot; (d) $H_2$-TPR profiles; (e) $O_2$-TPD profiles; (f) Raman spectra.

was around 1%. Compared with bare soot oxidation (R#1), both catalytic reaction (R#2 and R#3) exhibited better activity and $CO_2$ selectivity: $T_{50}$ (the temperature when soot conversion reaches 50%) shifted from 692 °C (R#1) to 619 °C (R#2) and 423 °C (R#3), and the selectivity ($S_a$) increased from 22% (R#1) to around 95% (R#2 and R#3). The differences of activity and selectivity between R#1, R#2 and R#3 could be visualized in Fig. 4. The distinct colors represent different kinds of isotopes. The outline of each peak was plotted by adding the concentration of various isotopes and then normalizing the total area. Therefore, the location of the peak on temperature axis indicates the activity; the area of purple, yellow, and blue regions indicates the selectivity; the area of blue, yellow and green reflects the water participation extent.

As shown in Scheme 1, bare soot oxidation follows Route A. The adsorption and dissociation of molecular oxygen on the surface of soot (A1) was the rate-limiting step. Thus SOCs formed with deficient AOS, such as carbonyl, ether and quinone groups and mainly released CO other than $CO_2$ [7–9]. But for catalytic soot oxidation, with the help of $Mn_2O_3$ catalyst, the energy barrier for dioxygen adsorption, activation and dissociation was greatly reduced. Thus much more AOS could participate in SOCs formation at lower temperatures. However, the quantity of AOS involved in SOCs formation per unit time was restricted by the contact condition. Compared with LC, the contact area between soot and $Mn_2O_3$ was larger under TC and the average distance for distant AOS to go through was shorter. Therefore, more close AOS would be generated (B1) and more distant AOS would reach their destination (C1 and C2) in unit time. With more AOS, not only SOCs formation but also their decomposition had been accelerated (B3). Hence as shown in Fig. 4, the normalized stacked concentration profiles of $CO_x$ under TC

was higher, sharper and appeared at lower temperatures than that under LC.

### 3.4. Soot oxidation under wet conditions

Before moving on to the soot oxidation reaction under wet conditions, it is necessary to point out that the reaction activity, selectivity and the extent of water participation would be discussed separately, as the influencing factors and results would be different. The proportions of labeling compound for each reaction have been summarized in Table 2.

#### 3.4.1. Bare soot oxidation

The addition of water slightly boosted bare soot combustion activity by comparing R#1 and R#4: as shown in Fig. 3(a), $T_{50}$ decreased from 692 ˚C (R#1) to 682 ˚C (R#4). The selectivity also improved from 22% to 30%. The distribution of $^{18}O$ isotope in $CO_x$ species offers more information about the role of water, as displayed in Fig. 5 and Table. 2. The appearance of $^{18}O$ isotope in CO ($P_m$, R#4) and $CO_2$ ($P_d$, R#4) indicated that water participate directly in bare soot oxidation, the precise percentage of which were 19.3% and 40.8% respectively. The difference between $P_m$ and $P_d$ suggested that water makes more contribution in the formation and decomposition of $CO_2$-generating SOCs than CO-generating SOCs.

Bare soot oxidation under wet conditions follows Route A and Route D in Scheme 1. Hence, the AOS were not only O* dissociated from dioxygen but also the ones with hydrogen (HO*). HO* could benefit the formation of carboxylic groups (D2), which is the least stable functional groups in SOCs [7–9] and hence promote the activity and $CO_2$ selectivity. However, in gas phase, $^{18}O$ accounted for 60% of total oxygen atoms ($P_r$), which was much higher than that in products. Thus, in bare soot oxidation, although water exhibited reactivity, it was lower compared with dioxygen, probably because of its harder adsorption on soot surface [46]. Moreover, during the reaction process, we observed the consumption of $O_2$ instead of $H_2O$, from which it could be inferred that although $H_2{}^{18}O$ served as an oxidant initially, the redundant H atoms had to be eliminated by dioxygen eventually. In general, water acted more likely as an accelerator to increase the total oxidation rate.

#### 3.4.2. Catalytic soot oxidation: the effect of contact condition

The presence of water in atmosphere accelerated the reaction rate in catalytic soot oxidation under both LC and TC conditions by comparing R#2 (LC, dry), R#3 (TC, dry), R#5 (LC, wet), and R#6 (TC, wet). As demonstrated in Fig. 3(b) and Table. 1, for LC, $T_{50}$ decreased from 619 ˚C (R#2) to 608 ˚C (R#5); for TC, it reduced from 423 ˚C (R#3) to 385 ˚C (R#6). The activity improvement of TC (38 ˚C) was larger than that of LC (11 ˚C). To avoid the influence of adsorption and desorption, soot-ISO were conducted under TC at 250 ˚C and 300 ˚C. As shown in Fig. 3(d), it was obvious that water accelerated soot oxidation at 300 ˚C. The selectivity remained around 95%. The activity improvement was mainly because of the more active HO* species dissociated from water and the faster regeneration of oxygen vacancies. As mentioned above, compared with SOCs that do not contain H atoms, carboxylic groups are less stable and easier to decompose. Hence, HO* could generate more active SOCs species (E2 in Scheme. 1). However, the decomposition of SOCs would produce both $CO_x$ (E3) and redundant H atoms (E4), which needed to be eliminated by dioxygen adsorbed on oxygen vacancies (E5). Under dry conditions, the formed O* occupied oxygen vacancies (B1), and only after they transport to soot surface (C1 & C2) could oxygen vacancies be released for another cycle. But under wet conditions, as the DFT calculation revealed, the desorption of $H_2O$ from the oxygen vacancy sites on catalyst was easier than that of $O_2$. Thus, with the help of surplus H atoms, the O*, especially the distant ones which require H to transport to the surface of catalyst (F1), could desorb as $H_2O$ (F2) instead of relocating to soot surface which required much more energy and regenerate the oxygen vacancies for dioxygen adsorption and dissociation (Fig. 4).

The participation of water was increased substantially comparing catalytic and bare soot oxidation. Moreover, the tighter contact, the greater increase. As shown in Table. 2, Figs. 5 and 6, $^{18}O$ accounted for only 29.2% of total oxygen atoms in products ($P_p$) for bare soot oxidation, but 67.8% and 83.4% for LC (R#5) and TC (R#6) respectively. Both $P_p$ were higher than that in reactants ($P_r$), which meant that $H_2O$ not only could be involved in catalytic soot oxidation directly but also was more active than $O_2$, which is contrary to bare soot oxidation. This improvement could be ascribed to the greater adsorption capacity of $H_2O$ than $O_2$. The adsorption capacity was determined by the relative partial pressure of $H_2O$ and $O_2$, and on the other hand, by the adsorption ability of $H_2O$ and $O_2$ on the surface of $Mn_2O_3$. As DFT calculation confirmed, on the top-site, the adsorption energy of $H_2O$ (−0.81 eV) was much stronger than that of $O_2$ (−0.60 eV). To elucidate the $P_p$ difference between LC and TC, it is quite necessary to discuss more detailed mechanism. The contact area between soot and $Mn_2O_3$ was much lager under TC than LC, hence TC relied more on close AOS (Route B & E) other than distant ones (Route C). In another word, under LC, the quantity of close AOS were not enough for SOCs formation, which required further participation of distant AOS transferring from the surface of catalyst. However, the mobility of various kinds of AOS (O* and HO*) are different and HO* with one more hydrogen should be less mobile compared with O*. Therefore, catalytic soot oxidation under LC utilized less HO* than TC and causing less water participation. It is also worth to note that O* could also be produced by the subsequent abstraction of H from HO*, which was not exhibited in Scheme 1. But the transport of such distant $^{18}O$* should not be influenced by contact condition.

#### 3.4.3. Catalytic soot oxidation: the effect of $O_2$ and $H_2O$ concentration

Although the DFT calculation confirmed the easier adsorption of $H_2O$ than $O_2$ on the surface of $Mn_2O_3$, the actual extent of participation could also be affected by the relative partial pressure of $O_2$ and $H_2O$ in gas phase. As listed in Table. 1, we conducted soot-TPO under two different atmosphere for both LC and TC modes. R#5 and R#6 were under lean $O_2$ atmosphere, where the labeled $^{18}O$ accounted for around 60% in reactants, while $P_r$ of lean $H_2O$ condition had decreased to about 6.5% (R#9 and R#10). As exhibited in Table. 2, although R#9 and R#10 were conducted in lean $H_2O$ atmosphere, the participation of water could not be omitted as $P_p$ for R#9 was 10.5% and that for R#10 reached 33.6%, which were both higher than $P_r$ apparently. The phenomena was consistent with lean $O_2$ atmosphere, indicating that although the gas partial pressure changed the surface coverage of $O_2$ and $H_2O$, the participation of $H_2O$ was still relative easier in subsequent reaction steps

**Table 2**
The proportions of labeling compound to total CO or $CO_2$, and the percentage of $^{18}O$ in reactants ($P_r$), CO ($P_m$), $CO_2$ ($P_d$) and all products ($P_p$).

| Reaction# | $P_r$ (%) | $C^{16}O$ (%) | $C^{18}O$ ($P_m$,%) | $C^{16}O_2$ | $C^{16}O^{18}O$ | $C^{18}O_2$ | $P_d$ (%) | $P_p$ (%) |
|---|---|---|---|---|---|---|---|---|
| R#4 | ~ 60 | 80.7 | 19.3 | 41.7 | 34.8 | 23.4 | 40.8 | 29.2 |
| R#5 | | 32.1 | 67.9 | 10.7 | 43.0 | 46.3 | 67.8 | 67.8 |
| R#6 | | 17.2 | 82.8 | 3.3 | 26.7 | 70.9 | 83.4 | 83.4 |
| R#7 | | 33.7 | 66.3 | 10.1 | 40.7 | 49.2 | 69.6 | 69.4 |
| R#8 | | 22.4 | 77.6 | 4.4 | 27.3 | 68.4 | 82.0 | 81.8 |
| R#9 | ~ 6.5 | 89.4 | 10.6 | 81.1 | 17.0 | 2.0 | 10.4 | 10.5 |
| R#10 | | 61.9 | 38.1 | 47.7 | 37.6 | 14.7 | 33.5 | 33.6 |

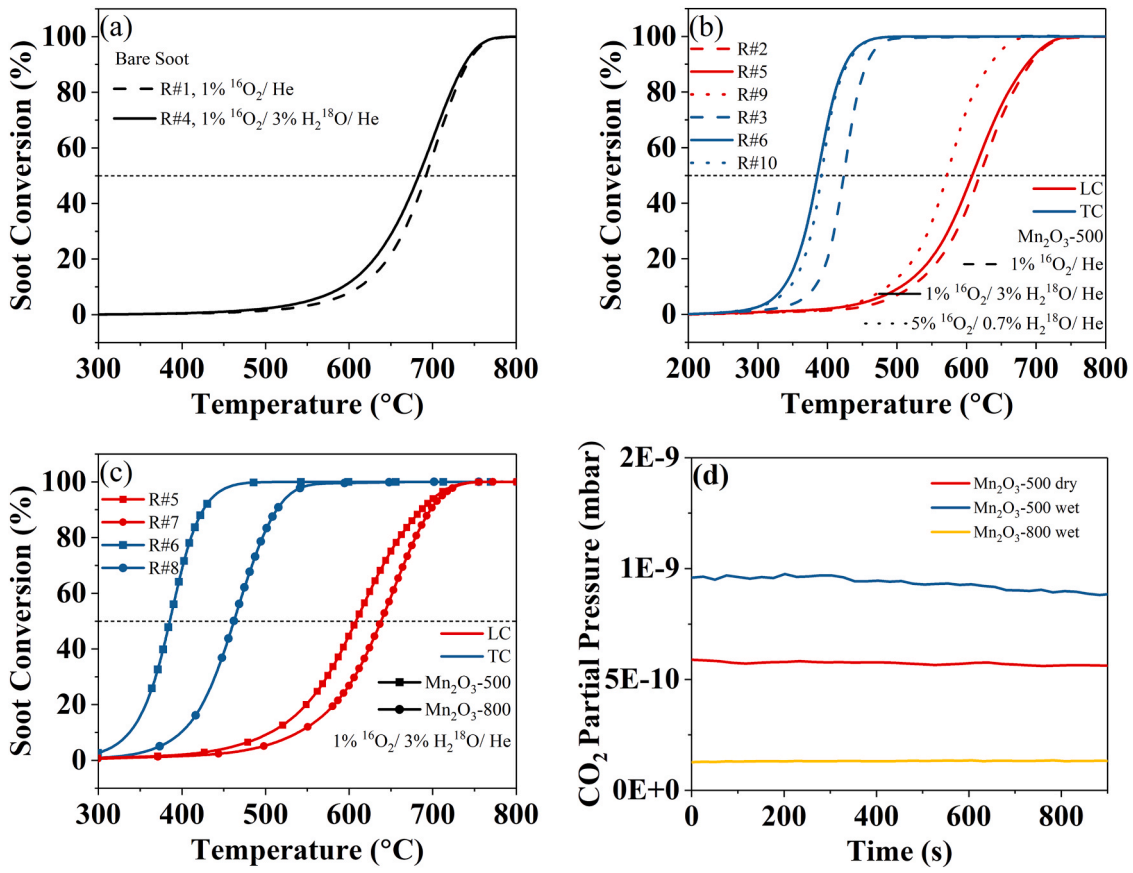


**Fig. 3.** The activity of soot oxidation. (a) Bare soot conversion profiles with (solid line) and without (dash line) water; (b) Catalytic soot oxidation with $Mn_2O_3$-500 catalyst in two contact modes (loose contact in red, tight contact in blue) and various reaction atmosphere; (c) Catalytic soot conversion profiles for catalysts with different redox properties; (d) Soot-ISO profiles under TC at 300 °C.

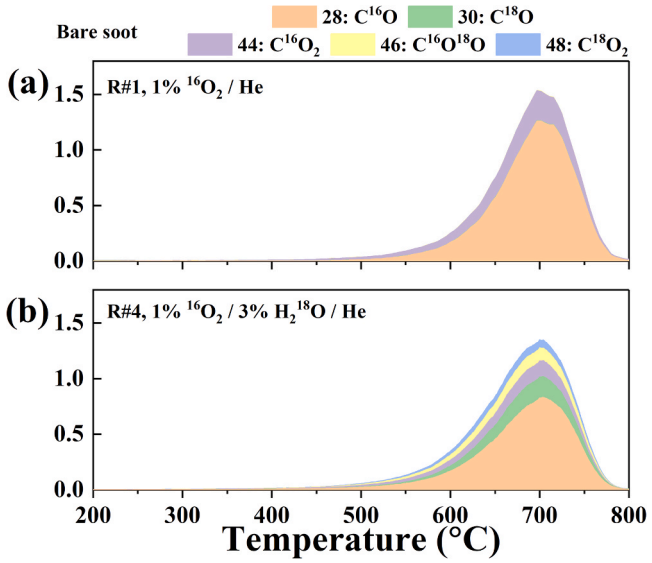


**Fig. 5.** The stacked concentration profiles of $C^{16}O$, $C^{18}O$, $C^{16}O_2$, $C^{16}O^{18}O$ and $C^{18}O_2$ for bare soot oxidation in dry and wet conditions. The total area has been normalized and is the same in each graph.

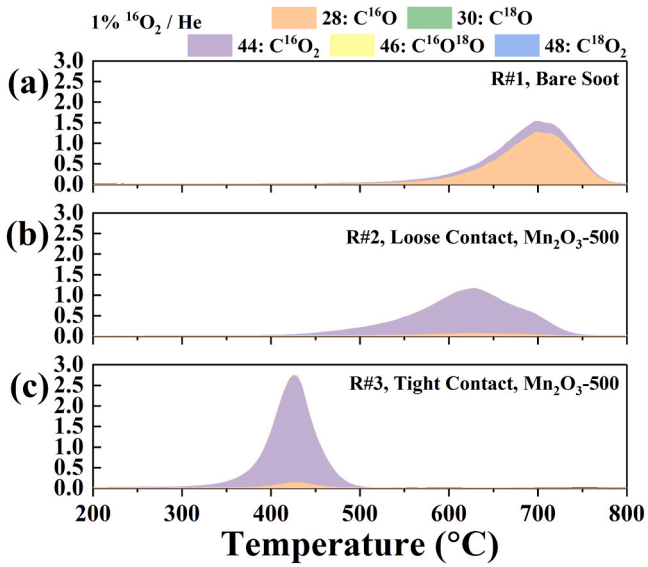


**Fig. 4.** The stacked concentration profiles of $C^{16}O$, $C^{18}O$, $C^{16}O_2$, $C^{16}O^{18}O$ and $C^{18}O_2$ for soot oxidation under dry conditions. The total area has been normalized and is the same in each graph.

(E2, E3).

As shown in Figs. 3(b) and 6, for LC, the increase of $O_2$ concentration decreased $T_{50}$ from 608 °C (R#5) to 572 °C (R#9); but for TC, the activity did not improve (R#6 and R#10). As we mentioned above, the contact condition influenced the quantity of AOS participated in SOCs formation and decomposition per unit time and distant AOS were mainly responsible under LC. So that more gas phase $O_2$ meant there would be more distant AOS reaching soot surface and forming SOCs. But for TC, which mainly utilized close AOS, the number of contact points between soot and catalyst generating close AOS did not vary despite of more $O_2$

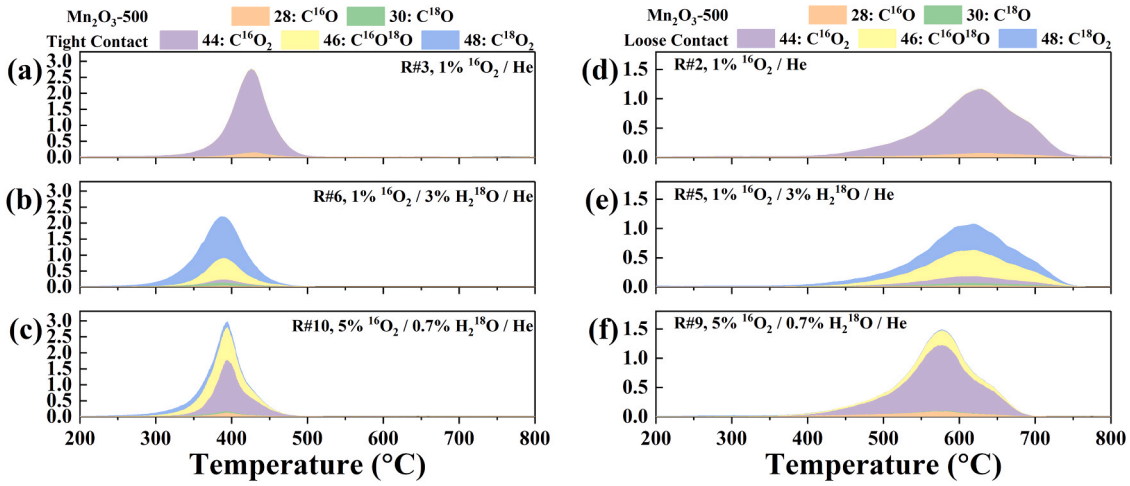


**Fig. 6.** The stacked soot-TPO profiles of $C^{16}O$, $C^{18}O$, $C^{16}O_2$, $C^{16}O^{18}O$ and $C^{18}O_2$ for catalytic soot oxidation under various reaction atmosphere. (a)-(c) were under TC, while (d)-(f) were under LC. The total area has been normalized and is the same in each graph.

supply. The influence of $O_2$ concentration on activity under TC was in agreement with other researchers [20].

### 3.4.4. *Catalytic soot oxidation: the effect of catalysts' redox property*

To further evaluate the effect of catalysts' redox property, $Mn_2O_3$-500 and $Mn_2O_3$-800 with different quantity of AOS-generating sites were prepared to conduct soot-TPO. As discussed previously, because $Mn_2O_3$-500 possessed more sites to produce AOS than $Mn_2O_3$-800, the activity of former one was better than the latter under both LC and TC. As listed in Table. 1 and shown in Fig. 7, under LC, $T_{50}$ for $Mn_2O_3$-800 was 638 ˚C, which was 30 ˚C higher than that of $Mn_2O_3$-500; under TC, both activity had increased as $T_{50}$ for $Mn_2O_3$-800 reached 462 ˚C and that for $Mn_2O_3$-500 reduced to 385 ˚C. However, just as shown in Table. 2, the participation of water were similar for $Mn_2O_3$-500 and $Mn_2O_3$-800. Under LC, both $P_p$ were around 68% (R#5 and R#7), while under TC, both were about 82% (R#6 and R#8). The results could be due to the increase of the quantity of AOS production sites did not change the adsorption and dissociation ability and probability of $O_2$ or $H_2O$ at each site. Moreover, after examining the concentration profiles of $C^{16}O_2$ and $H_2^{16}O$ for reaction R#8, we found their concentration mismatched in timing, that $H_2^{16}O$ was produced slightly later than $C^{16}O_2$. This phenomena supports our assumption on the reaction paths F1 and F2, via which the large-area catalyst's surface could act as a buffer for $H_2^{16}O$ production. The surplus H atoms migrate from the interface to catalyst surface (F1) and later recombined with surface oxygen to form $H_2^{16}O$ (F2) (Fig. 8).

## 3.5. *The reaction mechanism under wet condition*

So far, we try to summarize the reaction mechanism under wet condition and analyze the relationship between soot oxidation activity and water participation extent (Fig. 9), and summarize the influencing factors. In Fig. 9, the activity and water participation extent for each reaction are represented respectively by the size and the area of orange-colored wedge of each pie.

As shown in Scheme 1, there are three routes and three types of interfaces in soot oxidation under wet condition. Route D is a typical route for bare soot oxidation, where water can only be adsorbed and dissociated on the surface of soot. Although HO* can help the formation of less stable carboxylic groups, the surplus H atoms can hardly be depleted. Thus, the activity boost was limited and water participation extent remained low. Route E and F is dominant in catalytic soot oxidation. Water is adsorbed and dissociated on the soot-catalyst interface (E1). The derived HO* participate in the formation and decomposition of SOCs (E2 & E3), the redundant H atoms can eliminated by dioxygen adsorbed on oxygen vacancies (E5) or transferred to

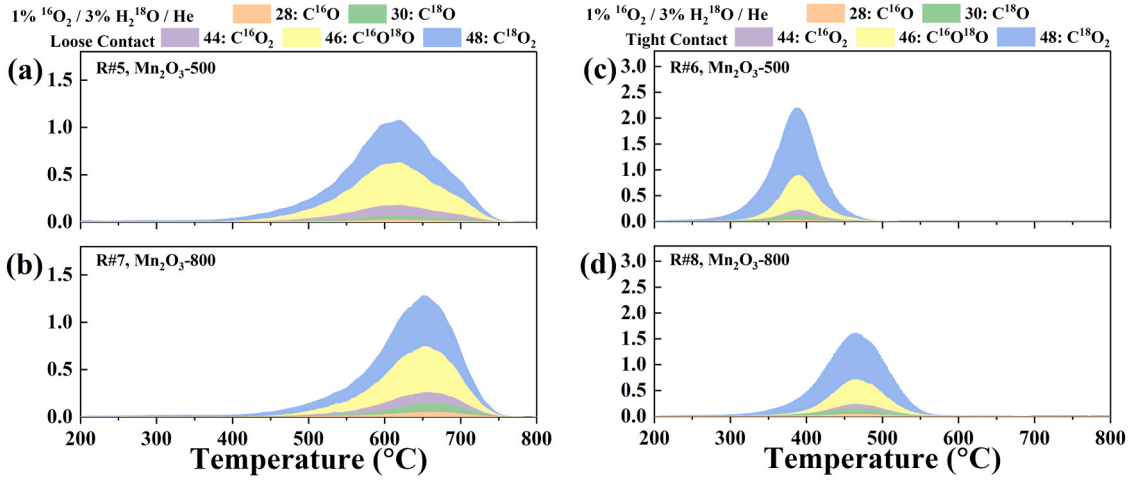


**Fig. 7.** The stacked soot-TPO profiles of $C^{16}O$, $C^{18}O$, $C^{16}O_2$, $C^{16}O^{18}O$ and $C^{18}O_2$ for catalytic soot oxidation, the catalysts of which contained different quantity AOS. (a)-(b) were under TC, (c)-(d) were under LC. The total area has been normalized and is the same in each graph.

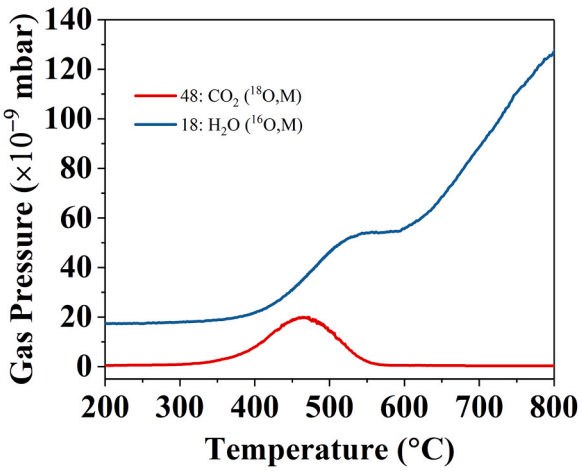


**Fig. 8.** The concentration profiles of $C^{16}O_2$ and $H_2^{16}O$ for reaction R#8.

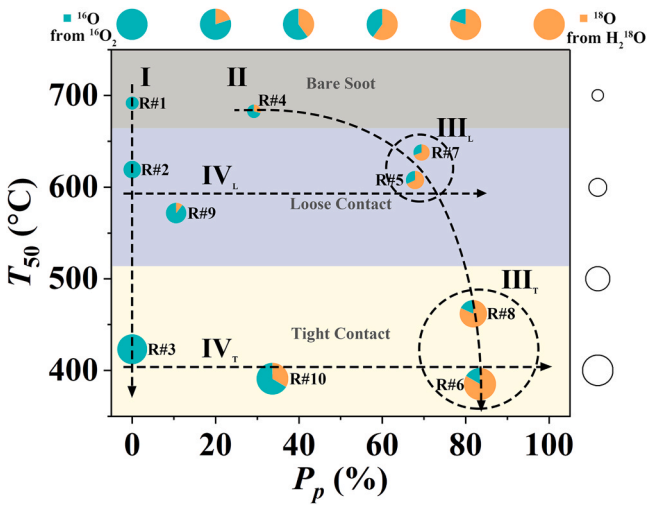


**Fig. 9.** The relationship between soot oxidation activity and water participation extent. The vertical axis is the temperature when soot conversion reaches 50% ($T_{50}$). The lower $T_{50}$, the larger pie chart, the better activity. The horizontal axis is the percentage of $^{18}O$ in all products ($P_p$). The more $^{18}O$, the larger orange-colored area in each pie chart.

catalyst surface at first (F1) and then be released (F2).

The soot oxidation activity reflects the quantity and decomposition ability of SOCs formed on soot surface per unit time. The former one is mainly determined by the AOS quantity reaching and reacting with free carbon sites on soot surface. Hence, if more AOS are generated on catalyst surface, and the distance between soot and catalyst is shorter, there would be more AOS to form SOCs. The quantity of AOS generated on catalyst surface is affected by the partial pressure of dioxygen and the redox property of catalyst. The distance between soot and catalyst is affected by the contact condition. Therefore, whether under dry (Line I in Fig. 9) or wet (Line II in Fig. 9) condition, the tighter contact, the better activity; the better catalyst's redox properties, the lower $T_{50}$ (Circle III in Fig. 9).

The participation extent of water reflects the competition between $H_2O$ and $O_2$ in soot oxidation reaction, namely the competition between Route B and Route E. The difference of relative mobility and activity of AOS (OH* and O*), and relative partial pressure both influence water participation extent. Therefore, the tighter contact, the more participation of HO* (Line II in Fig. 9); the larger relative partial pressure of $H_2O$ and $O_2$, the larger $P_p$ (Line IV in Fig. 9). But the quantity of AOS production sites of $Mn_2O_3$ catalysts will not affect their ability to adsorb $H_2O$ and $O_2$, hence did not influence water participation extent (Circle III in Fig. 9).

In general, the activity and water participation extent are both in connection with the AOS reaching and reacting with soot surface. But the activity is mainly determined by its quantity, while the water participation extent by the proportion of its sources. Hence the relationship between them was not straightforward.

In above discussion, we did not focus on the nature of AOS or the sites producing AOS because it is highly difficult to discriminate the specific sites or AOS. O* species could be $O^-$, $O_2^-$ or $O_2^{2-}$; while HO* species could be HO-, HOO-, or even HO radicals [47]. The generation sites could be oxygen vacancies, which were mostly considered, interstitial atoms, or other defects. Just in terms of oxygen vacancy, regrettably unlike $CeO_2$ [48], the Raman spectra of $Mn_2O_3$ could not be used to determine the extent of oxygen vacancies. Therefore the investigation of the nature and influence of AOS and their production sites would be a challenge to our future work.

## 4. Conclusion

In summary, isotopic experiments with heavy-oxygen water ($H_2{}^{18}O$) was designed to investigate the influence of water on soot oxidation. The extent of its participation was affected by catalysts, the contact condition between soot and catalyst, and the relative partial pressure of active gases, but not by the quantity of sites generating AOS on catalysts. Compared with dry conditions, the participation of water improved soot oxidation activity, because on one hand it could be adsorbed and dissociated easier than dioxygen on catalyst surface and form more active SOCs on soot surface, on the other hand it could boost the regeneration of oxygen vacancies. But during the reaction, the hydrogen atoms left by water still need to be eliminated by dioxygen. Hence despite that water participated in soot oxidation, in general it worked as an accelerator rather than oxidant. However, due to the complicated influencing factors of activity and water participation extent, there is no straightforward causality between them.

## CRediT authorship contribution statement

**Weinan Yang**: Designed and performed the experiment, Written the manuscript. **Ya Wang**: Did the DFT calculation. **Houlin Wang, Yani Zhang**: Participated in the results analysis and discussion. **Yue Peng, Junhua Li**: Supervised the project.

## Declaration of Competing Interest

The authors declare that they have no known competing financial interests or personal relationships that could have appeared to influence the work reported in this paper.

## Acknowledgment

This work was supported by the National Natural Science Foundation of China (21936005).

## References

[1] J.P. Neeft, M. Makkee, J.A. Moulijn, Diesel particulate emission control, Fuel Process. Technol. 47 (1) (1996) 1–69.
[2] C.A. Popelii, R.T. Burnett, M.J. Thun, E.E. Calle, D. Krewski, K. Ito, G.D. Thurston, Lung cancer, cardiopulmonary mortality, and long-term exposure to fine particulate air pollution, Jama 287 (9) (2002) 1132–1141.
[3] N.A. Janssen, G. Hoek, M. Simic-Lawson, P. Fischer, L. Van Bree, H. TenBrink, M. Keuken, R.W. Atkinson, H.R. Anderson, B. Brunekreef, et al., Black carbon as an additional indicator of the adverse health effects of airborne particles compared with $PM_{10}$ and $PM_{2.5}$, Environ. Health Perspect. 119 (12) (2011) 1691–1699.
[4] B.A. Van Setten, M. Makkee, J.A. Moulijn, Science and technology of catalytic diesel particulate filters, Catal. Rev. 43 (4) (2001) 489–564.
[5] L. Lisi, G. Landi, V. DiSarli, The issue of soot-catalyst contact in regeneration of catalytic diesel particulate filters: a critical review, Catalysts 10 (11) (2020) 1307.

[6] A. Mamakos, G. Martini, P. Dilara, Y. Drossinos, Feasibility of introducing particulate filters on gasoline direct injection vehicles. a cost benefit analysis., Tech. rep., European Commission Joint Research Center, 2011.

[7] P.E. Fanning, M.A. Vannice, A drifts study of the formation of surface groups on carbon by oxidation, Carbon 31 (5) (1993) 721–730.

[8] A. Setiabudi, M. Makkee, J.A. Moulijn, The role of $NO_2$ and $O_2$ in the accelerated combustion of soot in diesel exhaust gases, Appl. Catal. B: Environ. 50 (3) (2004) 185–194.

[9] J.L. Figueiredo, M. Pereira, M. Freitas, J. Orfao, Modification of the surface chemistry of activated carbons, Carbon 37 (9) (1999) 1379–1389.

[10] O.C. Williams, C. Sievers, Active oxygen species in heterogeneously catalyzed oxidation reactions, Appl. Catal. A: Gen. (2021), 118057.

[11] R.A. Ojifinni, N.S. Froemming, J. Gong, M. Pan, T.S. Kim, J. White, G. Henkelman, C.B. Mullins, Water-enhanced low-temperature CO oxidation and isotope effects on atomic oxygen-covered Au (111), J. Am. Chem. Soc. 130 (21) (2008) 6801–6812.

[12] C. Wang, X.-K. Gu, H. Yan, Y. Lin, J. Li, D. Liu, W.-X. Li, J. Lu, Water-mediated Mars-van Krevelen mechanism for CO oxidation on ceria-supported single-atom $Pt_1$ catalyst, ACS Catal. 7 (1) (2017) 887–891.

[13] J. Saavedra, H.A. Doan, C.J. Pursell, L.C. Grabow, B.D. Chandler, The critical role of water at the gold-titania interface in catalytic CO oxidation, Science 345 (6204) (2014) 1599–1602.

[14] X. Chen, G. He, Y. Li, M. Chen, X. Qin, C. Zhang, H. He, Identification of a facile pathway for dioxymethylene conversion to formate catalyzed by surface hydroxyl on $TiO_2$-based catalyst, ACS Catal. 10 (17) (2020) 9706–9715.

[15] Y. Li, X. Chen, C. Wang, C. Zhang, H. He, Sodium enhances $Ir/TiO_2$ activity for catalytic oxidation of formaldehyde at ambient temperature, ACS Catal. 8 (12) (2018) 11377–11385.

[16] R. Schneider, D. Kiessling, G. Wendt, Cordierite monolith supported perovskite-type oxides–catalysts for the total oxidation of chlorinated hydrocarbons, Appl. Catal. B: Environ. 28 (3–4) (2000) 187–195.

[17] Q. Dai, X. Wang, G. Lu, Low-temperature catalytic combustion of trichloroethylene over cerium oxide and catalyst deactivation, Appl. Catal. B: Environ. 81 (3–4) (2008) 192–202.

[18] X. Weng, Q. Meng, J. Liu, W. Jiang, S. Pattisson, Z. Wu, Catalytic oxidation of chlorinated organics over lanthanide perovskites: effects of phosphoric acid etching and water vapor on chlorine desorption behavior, Environ. Sci. Technol. 53 (2) (2018) 884–893.

[19] J.M. Christensen, J.-D. Grunwaldt, A.D. Jensen, Effect of $NO_2$ and water on the catalytic oxidation of soot, Appl. Catal. B: Environ. 205 (2017) 182–188.

[20] R. Zhang, W. Yang, J. Xue, B. Chen, The influence of $O_2$, hydrocarbons, CO, $H_2$, $NO_x$, $SO_2$, and water vapor molecules on soot combustion over $LaCoO_3$ perovskite, Catal. Lett. 132 (1) (2009) 10–15.

[21] M. Jeguirim, V. Tschamber, J. Brilhac, P. Ehrburger, Oxidation mechanism of carbon black by $NO_2$: effect of water vapour, Fuel 84 (14–15) (2005) 1949–1956.

[22] C. Arnal, M. Alzueta, A. Millera, R. Bilbao, Influence of water vapor addition on soot oxidation at high temperature, Energy 43 (1) (2012) 55–63.

[23] Y. Gao, A. Duan, S. Liu, X. Wu, W. Liu, M. Li, S. Chen, X. Wang, D. Weng, Study of $ag/Ce_xNd_{1-x}O_2$ nanocubes as soot oxidation catalysts for gasoline particulate filters: balancing catalyst activity and stability by Nd doping, Appl. Catal. B: Environ. 203 (2017) 116–126.

[24] A.M. Hernández-Giménez, D. Lozano-Castelló, A. Bueno-López, Effect of $CO_2$, $H_2O$ and $SO_2$ in the ceria-catalyzed combustion of soot under simulated diesel exhaust conditions, Appl. Catal. B: Environ. 148 (2014) 406–414.

[25] C.S. Park, M.W. Lee, J.H. Lee, E.J. Jeong, S.H. Lee, J.W. Choung, C.H. Kim, H. C. Ham, K.-Y. Lee, Promoting effect of $H_2O$ over macroporous Ce-Zr catalysts in soot oxidation, Mol. Catal. 474 (2019), 110416.

[26] W. Yang, S. Wang, K. Li, S. Liu, L. Gan, Y. Peng, J. Li, Highly selective $\alpha$-$Mn_2O_3$ catalyst for cGPF soot oxidation: surface activated oxygen enhancement via selective dissolution, Chem. Eng. J. 364 (2019) 448–451.

[27] H. Xu, N. Yan, Z. Qu, W. Liu, J. Mei, W. Huang, S. Zhao, Gaseous heterogeneous catalytic reactions over Mn-based oxides for environmental applications: a critical review, Environ. Sci. Technol. 51 (16) (2017) 8879–8892.

[28] J. He, S.-Y. Chen, W. Tang, Y. Dang, P. Kerns, R. Miao, B. Dutta, P.-X. Gao, S. L. Suib, Microwave-assisted integration of transition metal oxide nanocoatings on manganese oxide nanoarray monoliths for low temperature CO oxidation, Appl. Catal. B: Environ. 255 (2019), 117766.

[29] L. Pahalagedara, D.A. Kriz, N. Wasalathanthri, C. Weerakkody, Y. Meng, S. Dissanayake, M. Pahalagedara, Z. Luo, S.L. Suib, P. Nandi, et al., Benchmarking of manganese oxide materials with CO oxidation as catalysts for low temperature selective oxidation, Appl. Catal. B: Environ. 204 (2017) 411–420.

[30] K. Frey, V. Iablokov, G. Sáfrán, J. Osán, I. Sajó, R. Szukiewicz, S. Chenakin, N. Kruse, Nanostructured $MnO_x$ as highly active catalyst for CO oxidation, J. Catal. 287 (2012) 30–36.

[31] X. Wang, Y. Liu, Y. Zhang, T. Zhang, H. Chang, Y. Zhang, L. Jiang, Structural requirements of manganese oxides for methane oxidation: XAS spectroscopy and transition-state studies, Appl. Catal. B: Environ. 229 (2018) 52–62.

[32] Y.-F. Han, K. Ramesh, L. Chen, E. Widjaja, S. Chilukoti, F. Chen, Observation of the reversible phase-transformation of $\alpha$-$Mn_2O_3$ nanocrystals during the catalytic combustion of methane by in situ Raman spectroscopy, J. Phys. Chem. C 111 (7) (2007) 2830–2833.

[33] Y. Wang, S. Aghamohammadi, D. Li, K. Li, R. Farrauto, Structure dependence of $Nb_2O_{5-x}$ supported manganese oxide for catalytic oxidation of propane: enhanced oxidation activity for $MnO_x$ on a low surface area $Nb_2O_{5-x}$, Appl. Catal. B: Environ. 244 (2019) 438–447.

[34] J. Wang, J. Li, C. Jiang, P. Zhou, P. Zhang, J. Yu, The effect of manganese vacancy in birnessite-type $MnO_2$ on room-temperature oxidation of formaldehyde in air, Appl. Catal. B: Environ. 204 (2017) 147–155.

[35] Z. Sihaib, F. Puleo, J. Garcia-Vargas, L. Retailleau, C. Descorme, L. Liotta, J. Valverde, S. Gil, A. Giroir-Fendler, Manganese oxide-based catalysts for toluene oxidation, Appl. Catal. B: Environ. 209 (2017) 689–700.

[36] G. Li, N. Li, Y. Sun, Y. Qu, Z. Jiang, Z. Zhao, Z. Zhang, J. Cheng, Z. Hao, Efficient defect engineering in Co-Mn binary oxides for low-temperature propane oxidation, Appl. Catal. B: Environ. 282 (2021), 119512.

[37] S.C. Kim, W.G. Shim, Catalytic combustion of VOCs over a series of manganese oxide catalysts, Appl. Catal. B: Environ. 98 (3–4) (2010) 180–185.

[38] T. Liu, Q. Li, Y. Xin, Z. Zhang, X. Tang, L. Zheng, P.-X. Gao, Quasi free K cations confined in hollandite-type tunnels for catalytic solid (catalyst)-solid (reactant) oxidation reactions, Appl. Catal. B: Environ. 232 (2018) 108–116.

[39] D. Jampaiah, V.K. Velisoju, P. Venkataswamy, V.E. Coyle, A. Nafady, B.M. Reddy, S.K. Bhargava, Nanowire morphology of mono-and bidoped $\alpha$-$MnO_2$ catalysts for remarkable enhancement in soot oxidation, ACS Appl. Mater. Interfaces 9 (38) (2017) 32652–32666.

[40] G. Kresse, J. Hafner, Ab initio molecular-dynamics simulation of the liquid-metal-amorphous-semiconductor transition in germanium, Phys. Rev. B 49 (20) (1994) 14251.

[41] G. Kresse, D. Joubert, From ultrasoft pseudopotentials to the projector augmented-wave method, Phys. Rev. B 59 (3) (1999) 1758.

[42] J.P. Perdew, K. Burke, M. Ernzerhof, Generalized gradient approximation made simple, Phys. Rev. Lett. 77 (18) (1996) 3865.

[43] S. Dudarev, G. Botton, S. Savrasov, C. Humphreys, A. Sutton, Electron-energy-loss spectra and the structural stability of nickel oxide: an LSDA+U study, Phys. Rev. B 57 (3) (1998) 1505.

[44] L. Wang, T. Maxisch, G. Ceder, Oxidation energies of transition metal oxides within the GGA+U framework, Phys. Rev. B 73 (19) (2006), 195107.

[45] Y.-F. Han, F. Chen, Z.-Y. Zhong, K. Ramesh, E. Widjaja, L.-W. Chen, Synthesis and characterization of $Mn_3O_4$ and $Mn_2O_3$ nanocrystals on SBA-15: Novel combustion catalysts at low reaction temperatures, Catal. Commun. 7 (10) (2006) 739–744.

[46] A. Allouche, Y. Ferro, Dissociative adsorption of small molecules at vacancies on the graphite (0001) surface, Carbon 44 (15) (2006) 3320–3327.

[47] R. Caporali, S. Chansai, R. Burch, J.J. Delgado, A. Goguet, C. Hardacre, L. Mantarosie, D. Thompsett, Critical role of water in the direct oxidation of CO and hydrocarbons in diesel exhaust after treatment catalysis, Appl. Catal. B: Environ. 147 (2014) 764–769.

[48] X. Lin, S. Li, H. He, Z. Wu, J. Wu, L. Chen, D. Ye, M. Fu, Evolution of oxygen vacancies in $MnO_x$-$CeO_2$ mixed oxides for soot oxidation, Appl. Catal. B: Environ. 223 (2018) 91–102.